Remote Sensing Letters

ISSN: 2150-704X (Print) 2150-7058 (Online) Journal homepage: http://www.tandfonline.com/loi/trsl20

Machine learning-based temporal mixture analysis of hypertemporal Antarctic sea ice data

Junhwa Chi, Hyun-Cheol Kim & Sung-Ho Kang

To cite this article: Junhwa Chi, Hyun-Cheol Kim & Sung-Ho Kang (2016) Machine learning-based temporal mixture analysis of hypertemporal Antarctic sea ice data, Remote Sensing Letters, 7:2, 190-199, DOI: 10.1080/2150704X.2015.1121300

To link to this article: http://dx.doi.org/10.1080/2150704X.2015.1121300

Published online: 03 Dec 2016.

REMOTE SENSING LETTERS, 2016
VOL. 7, NO. 2, 190–199
http://dx.doi.org/10.1080/2150704X.2015.1121300

Taylor & Francis
Taylor & Francis Group

Machine learning-based temporal mixture analysis of hypertemporal Antarctic sea ice data

Junhwa Chi, Hyun-Cheol Kim and Sung-Ho Kang

Division of Polar Ocean Environment, Korea Polar Research Institute, Incheon, Korea

ABSTRACT

Hypertemporal image (HTI) is often used to exploit the seasonal characteristics of environmental phenomena such as sea ice concentration (SIC). However, it is difficult to analyse the long-term time series acquired at high temporal frequencies and over extensive areas. This study performed temporal mixture analysis (TMA), which is algebraically similar to spectral mixture analysis (SMA), but occurs in the time domain instead of the spectral domain. TMA was used to investigate the temporal characteristics of Antarctic sea ice. Because endmember (EM) selection is critical to the success of both SMA and TMA, it is important to select proper EMs from large quantities of HTI. In this study, a machine learning (ML) technique is incorporated in identifying EMs without prior information to address the limitations of previous research. A fully linear mixing model was then implemented in an attempt to produce more robust and physically meaningful abundance estimates. Experiments that quantitatively and qualitatively evaluated the proposed approaches were conducted. A TMA of high-temporal-dimensional data provides a unique summary of long-term Antarctic sea ice and noise-whitened reconstruction images via inverse processing. Furthermore, comparisons of regional sea ice fractions from experimental results enhance the understanding of the overall Antarctic sea ice changes.

ARTICLE HISTORY
Received 5 August 2015
Accepted 10 November 2015

1. Introduction

Changes in human behaviour and increases in greenhouse gases have been the main drivers of the observed global warming. An increasing amount of attention worldwide has thus been given to various studies of climate change. Researchers expect that climate change will be more rapid and severe in the polar regions than it will be at temperate latitudes. Thus, the sensitivity of sea ice to temperature is a barometer for general trends in global climate (Parry 2007). Compared with in situ measurements, remotely sensed data from various platforms better enable the efficient and regular assessment of large, inaccessible areas. Remote sensing (RS) data thus allow important ecosystem functions to be efficiently mapped and monitored.

Optical RS sensors typically record radiation reflected from a ground target over a continuous range of contiguous bands. Hyperspectral sensors, which often acquire data in hundreds of narrow bands, provide better data for identifying materials than do multispectral sensors. However, hyperspectral imaging (HSI) is limited in its capacity to effectively monitor the Arctic

CONTACT Hyun-Cheol Kim kimhc@kopri.re.kr

and the Antarctic due to narrow swaths, long revisit cycles and severe weather conditions. From a different perspective, a set of long-term RS data might capture seasonal profiles and track changes that can be used to monitor and map the temporal dynamics of land cover (DeFries, Hansen, and Townshend 2000; Lobell and Asner 2004; Yang et al. 2012). Throughout this paper, the term 'hypertemporal image' (HTI) refers to time series-based RS data acquired at high frequencies.

Many analysis techniques for multispectral and hyperspectral data have been investigated in the spectral domain (Plaza et al. 2004; Bioucas-Dias et al. 2012). The most popular analysis technique in the RS community is classification, wherein each pixel of the image is assigned to a discrete class. Another popular technique, called spectral unmixing or spectral mixture analysis (SMA), decomposes the pixels into a collection of individual pure spectral signatures, which are referred to as 'endmembers' (EMs), at sub-pixel levels (Keshava and Mustard 2002). Temporal mixture analysis (TMA) is an extension of SMA of HSI to the temporal domain that provides a unique summary of HTIs and describes the seasonal characteristics, rather than radiometric characteristics, of ground cover (Piwowar, Peddle, and Ledrew 1998; Piwowar 2008; Haibo and Ziwei 2011; Yang et al. 2012). Although SMA has been extensively investigated using HSI, few studies have examined TMA because this approach is still in its infancy (Piwowar, Peddle, and Ledrew 1998). Piwowar, Peddle, and Ledrew (1998) first investigated TMA by analysing long-term temporal RS data that were generated using 9 years of Arctic sea ice concentration (SIC) data. The authors defined temporal EMs using simple statistics, computed fractional abundances using a linear mixing model, and then derived the temporal characteristics of the Arctic SIC. This approach was demonstrated in monitoring the variability of the Antarctic SIC in Haibo and Ziwei (2011). Following this research, several studies have applied TMA to other various applications. DeFries, Hansen, and Townshend (2000) applied a linear mixture model to derive globally continuous fields for vegetation characteristics using multiple years of AVHRR (Advanced Very High Resolution Radiometer) data. In Lobell and Asner (2004), a perpendicular vegetation index of Moderate Resolution Imaging Spectroradiometer (MODIS) time series data and linear unmixing were used to estimate sub-pixel fractions of land-cover types. Next, Yang et al. (2012) proposed a TMA method to compute impervious surface area fractions in Japan using multi-year MODIS normalized difference vegetation index (NDVI) data.

Identifying an appropriate set of EMs is the most critical part of both SMA and TMA (Keshava and Mustard 2002; Plaza et al. 2004). Piwowar, Peddle, and Ledrew (1998) identified temporal EMs using monthly Arctic SIC data derived from a scanning multi-channel microwave radiometer (SMMR) performed using a Nimbus platform and a purification formula. In this approach, mean, median, maximum and minimum statistics are used to derive pure temporal EM spectra from a sample set of image spectra. However, this method may not properly capture the seasonal characteristics of sea ice because monthly data provide insufficient temporal information, and the temporal EMs generated by the purification process are not always collected on the same scale as the image data. Inaccurate temporal EMs might introduce many reconstruction errors. In this paper, machine learning (ML) techniques were used for TMA of Antarctic SIC to provide unique and summarized information of long-term time series. First, daily SIC data, which are similar to HSI but are in a different domain, were used to better seasonally characterize the Antarctic sea ice. Second, due to a lack of prior information on sea ice seasonality, an ML-based endmember extraction (EE) algorithm was applied to generate a collection of pure temporal signatures. Next, quantitative and qualitative experiments were performed and discussed to evaluate the proposed approaches.

2. Methodology

2.1. *Hypertemporal sea ice concentration data*

Based on the assumption that SIC data[1] provided by NSIDC (National Snow and Ice Data Center) guarantee the data quality at a global scale, 36 years of SIC data from 1979 to 2014 over the Antarctic were used in this study. The data were generated from the SMMR on Nimbus 7 satellite, Special Sensor Microwave/Imagers (SSM/Is) on the Defense Meteorological Satellite Program (DMSP) -F8, -F11 and -F13 satellites and the Special Sensor Microwave Imager/Sounder (SSMIS) on DMSP-F17 satellites, at 25-km spatial resolution in the polar stereographic projection. The NASA Team algorithm was applied to these data sets to analyse the time series data acquired from different sensors (Cavalieri et al. 1996). SIC data from 1978 to 1987 were collected every other day; these data gaps were filled using linear interpolation to generate consistent daily time series data throughout the time period.

2.2. *Temporal mixture analysis*

Most pixels from RS data comprise several distinct materials due to resolution trade-off, intimate mixtures and multiple interferences, among other concerns. SMA assumes that the surface is dominated by a small number of such substances and can be modelled by representing the substances at sub-pixel levels (Keshava and Mustard 2002). The main idea underlying TMA of HTIs is rooted in SMA. TMA also assumes that the time series consist of several temporal components that represent the seasonal characteristics of the substances. Two general steps were employed to address the mixing problems: 1) identifying temporally unique signatures of pure components, which are referred to as temporal EMs and 2) unmixing each pixel in the time series images as a linear or non-linear combination of EM fractional abundances. Because temporal EMs in the SIC time series typically correspond to seasonal sea ice signatures, TMA can quantitatively estimate the SIC each season as a unique and informative summary of the long-term time series.

Because of its robustness and ease of implementation, linear unmixing is often used to resolve mixing phenomena. Linear mixing models for TMA assume that the temporal trajectories of seasonal sea ice are linearly independent and that the pixels in the images lie in linear spaces. The set of HTI matrices is denoted as follows: $[X : \boldsymbol{x_i}, i = 1, 2, \cdots, N] \in \mathrm{R}^D$, with temporal dimension D and number of samples N. Let x_i be the i-th daily trajectory of HTI. The temporal spectrum $\boldsymbol{x}$ can be modelled as a linear combination of several temporal EM vectors $\left[\mathrm{E} : \boldsymbol{e}_j, j = 1, 2, \cdots, q\right]$, where q is the number of temporal EMs. Each temporal spectrum at pixel $\boldsymbol{x}_i$ can be expressed by $\sum_{j=1}^{q} a_{i,j}\boldsymbol{e}_j + \omega$, where $a_{i,j}$ is a scalar value that represents the fractional abundance of the temporal EM vector $\boldsymbol{e}_j$ at pixel $\boldsymbol{x}_i$, and ω denotes additive variability (e.g., noise, measurement or model errors). In practice, fully constrained least squares unmixing is typically used to estimate physically meaningful abundances with two constraints for each HTI pixel x_i: 1) non-negative: $a_{i,j} \geq 0; \forall a_{i,j} : 1 \leq j \leq q$ and 2) sum-to-one: $\sum_{j=1}^{q} a_{i,j} = 1$, which are defined as later (Heinz and Chang 2001).

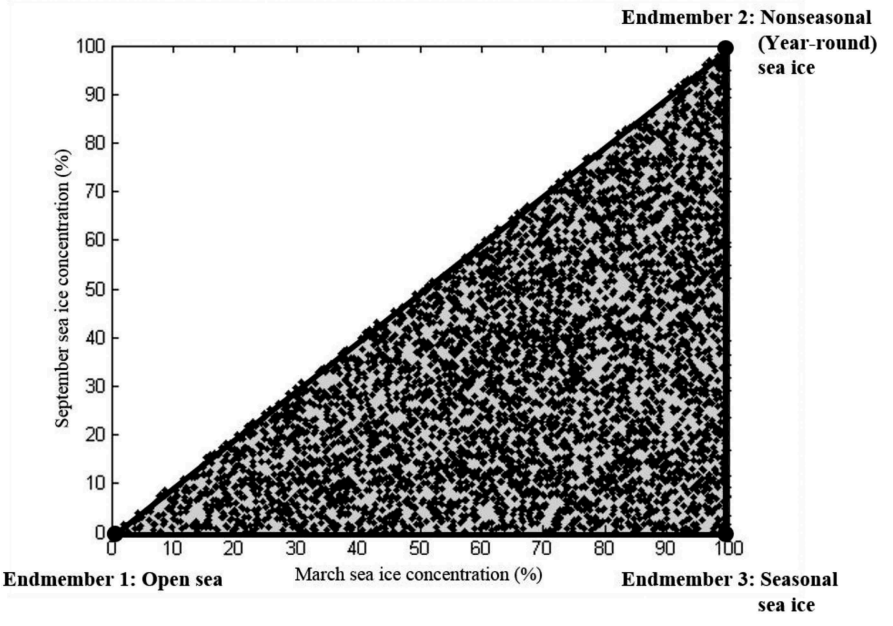

Figure 1. Basic definition of the temporal endmembers (Piwowar, Peddle, and Ledrew 1998).

For example, Figure 1 illustrates the effects of mixing on the multi-temporal SIC using three temporal EMs: 1) the open sea (sea ice free in both March and September), 2) non-seasonal sea ice (100% sea ice cover in both March and September) and 3) seasonal sea ice (100% SIC in March and 0% in September) signatures (Piwowar, Peddle, and Ledrew 1998). Because the mixture points in the two temporal bands shown in Figure 1 are spread along the lines between the EMs, the corresponding fractional abundances, which are related to 'physical' quantities of the EMs, can be computed.

2.3. *Endmember extraction*

The most crucial task in both SMA and TMA is identifying an appropriate set of EMs to use in the modelling of at-sensor pixel spectra or temporal trajectories through a linear combination of the EMs. In this study, a Neyman–Pearson detection-theory-based eigenthreshold method, referred to as the Harsanyi–Farrand–Chnag (HFC) method, was used to determine the number of EMs in hypertemporal data without prior information. This method first computes the sample correlation and covariance matrices, and then determines the difference between the corresponding eigenvalues (Harsanyi, Farrand, and Chang 1993). Because image-derived EMs have the advantage of being collected under the same conditions as the RS data, an ML-based EE algorithm was used for the HTI of the SIC. Over the past decade, many ML algorithms have been proposed by the hyperspectral RS community to identify image EMs. Assuming that pure or extreme signatures are EMs, the notion of geometric convexity is natural and logical. Thus, this approach is the most popular and is used to develop a wide range of algorithms.

The N-FINDR algorithm developed by Winter (1999) was used in this study because studies show that it is promising for many HSI unmixing applications (Winter 1999; Plaza et al. 2004; Chi and Crawford 2014). This automated technique attempts to identify a set of

vertices that can be specified by EMs. It uses the simplex of maximum volume spanned by the EMs as a major criterion and is based on the assumption that the volume defined by a simplex spanned by the purest pixels is greater than any other volume defined by any other combination of pixels. If HSI or HTI data are distributed over a convex space, this operation can be performed quickly and in a relatively straightforward manner. N-FINDR arbitrarily selects initial seed points (EM candidates), and the volume of the resulting simplex spanned by the seed points is computed as follows: $V(\boldsymbol{e}_1, \boldsymbol{e}_2, \cdots, \boldsymbol{e}_q) = \left|\det\left(\begin{bmatrix} 1 & 1 & \cdots & 1 \\ \boldsymbol{e}_1 & \boldsymbol{e}_2 & \cdots & \boldsymbol{e}_q \end{bmatrix}\right)\right|/(q-1)!$. The volume is evaluated for each pixel to replace each EM position as a new simplex vertex until no larger simplex is found, as follows: $\arg \max_{(\boldsymbol{e}_1, \boldsymbol{e}_2, \cdots, \boldsymbol{e}_q)} V(\boldsymbol{e}_1, \boldsymbol{e}_2, \cdots, \boldsymbol{e}_q)$. N-FINDR requires dimensionality reduction because the matrix $\begin{bmatrix} 1 & 1 & \cdots & 1 \\ \boldsymbol{e}_1 & \boldsymbol{e}_2 & \cdots & \boldsymbol{e}_q \end{bmatrix}$ must be a square matrix for its determinant to exist (Winter 1999). In this study, the maximum noise fraction (MNF) transform proposed by Green et al. (1988) was used. The MNF was first developed as an alternative to principal component analysis (PCA) to address data variance issues that are not always related to image quality, because principal components are not necessarily ordered by image quality. The MNF transformation was derived as a PCA analogue and includes all of the PCA properties, but it utilizes a signal-to-noise ratio to measure image quality, which produces the equivalent of a noise-whitened PCA (Cheriyadat and Bruce 2003).

3. Experimental results

Using the HFC virtual dimensionality algorithm for hypertemporal SIC data acquired from 1979 to 2014 with various false alarm probabilities $\left(P_F = 10^{-1}, 10^{-2}, 10^{-3}, 10^{-4}, 10^{-5}\right)$ produced the same virtual dimensionality estimates (Harsanyi, Farrand, and Chang 1993). Therefore, the number of potential temporal EMs was determined to be 9. The N-FINDR algorithm identified the representative nine temporal EMs, which include open ocean (E1), year-round sea ice (E2) and seven seasonal sea ice signatures (E3–E9) and are shown in Figure 2. Next, the corresponding fractional abundances associated with the temporal EMs were created using a fully constrained linear mixing model (see Figure 3). The fractional abundance maps of the extracted temporal EMs represent the spatial distribution of sea ice during a particular season and provide a quick summary of the temporal characteristics of hypertemporal SIC data for each year. These data also indicate that the HTI can be reconstructed via the inverse process of pixel unmixing. Although a combination of the temporal EMs and the corresponding fractions does not always ensure perfect reconstruction, it can be used, to a certain extent, to create reference images that do not contain anomalies from other unexpected environmental factors and that mitigates the impact of processing error noise.

3.1. *Reconstruction image comparison*

In SMA, unmixing results are typically tested in two ways: 1) using the spectral angle distance between the extracted EMs and reference spectra acquired from a spectral library or field data and 2) using pixel reconstruction error. It is relatively easy to obtain ground reflectance information for SMA (Keshava and Mustard 2002; Plaza et al. 2004;

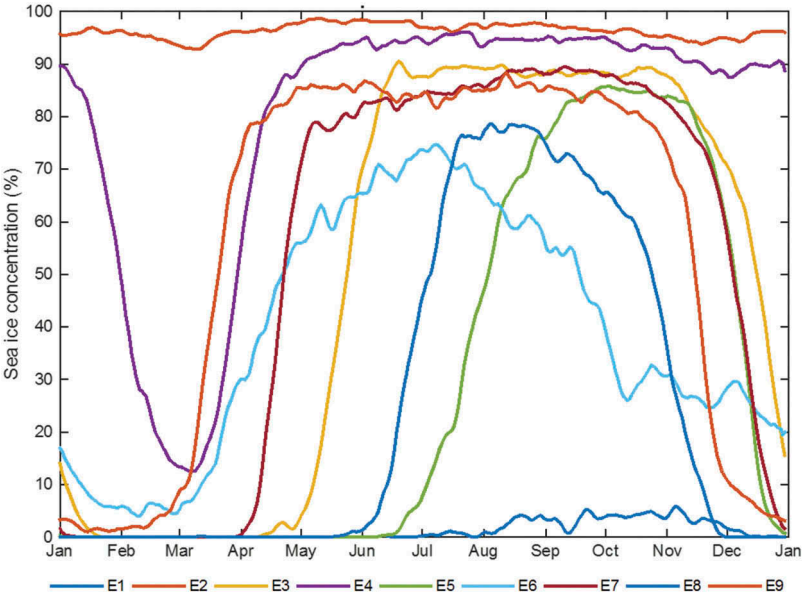

Figure 2. Extracted temporal endmembers (E1: open sea; E2: year-round sea ice; and E3–E9: seasonal sea ice signatures) showing the variation in sea ice concentration throughout the year.

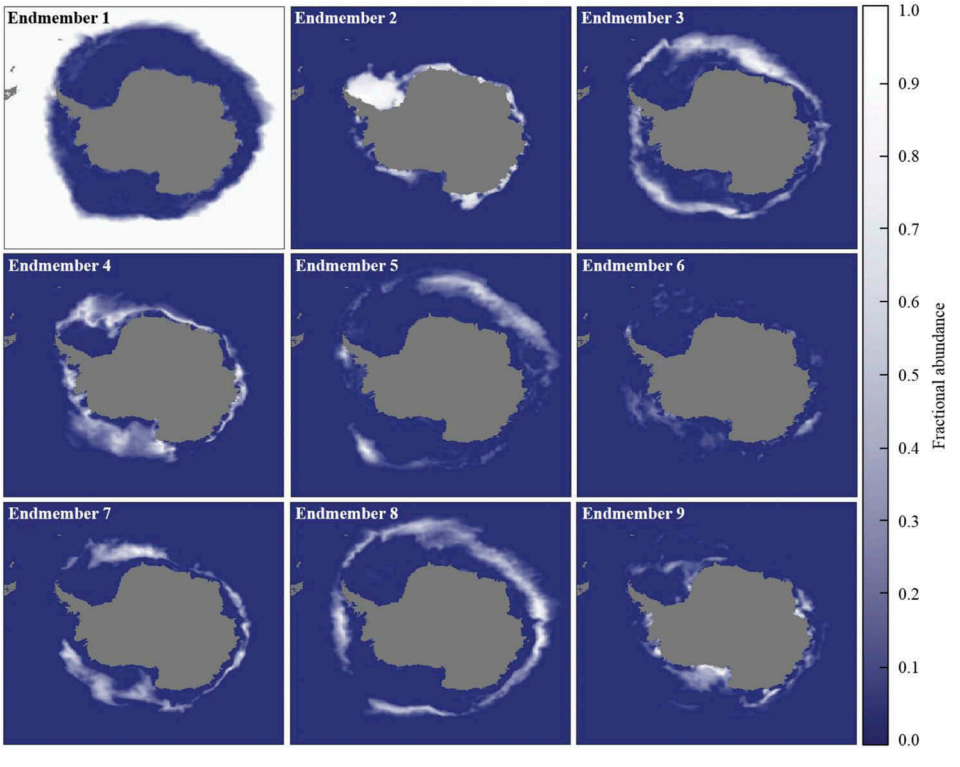

Figure 3. Fractional abundance maps of temporal endmembers E1–E9.

Bioucas-Dias et al. 2012); however, it is challenging to do so for TMA because seasonality reference data for time series do not exist. Therefore, it is not possible to use distance-based similarity comparison with reference spectra to evaluate TMA results. Instead, root mean square error (RMSE) was used to provide an overall 'pixel-by-pixel' difference between the original and reconstructed SIC images.

Figure 4 shows reconstructions of 2014 HTI using three RMSE values: 1) the best fit (Figure 4(a)), 2) the worst fit (Figure 4(b)) and 3) the case most statistically similar to the mean (Figure 4(c)). The reconstructed images did not capture the detailed variability in the local areas as shown in Figure 4; however, they generally exhibited better visual consistency with the original images. Because Figure 4(a) shows a good RMSE, the reconstructed image appears to have been adequately reconstructed both visually and statistically. However, Figure 4(b) especially shows low accuracy and low fidelity with the original image. This is because the representative EMs might not adequately model the areas where sea ice might be melting. Notably, little success was achieved using representative seasonal sea ice data from the previous 36 years to inform the modelling of areas that might be associated with other environmental (climatological) factors.

3.2. *Regional comparison*

The Arctic SIC exhibits a long-term negative trend; however, the overall Antarctic sea ice has been expanding for decades (Screen 2011; Parkinson and Cavalieri 2012). Antarctic sea ice set record highs from 2012 to 2014, even though average Antarctic surface temperatures were close to the highest temperatures observed. Interestingly, however, SICs exhibit great

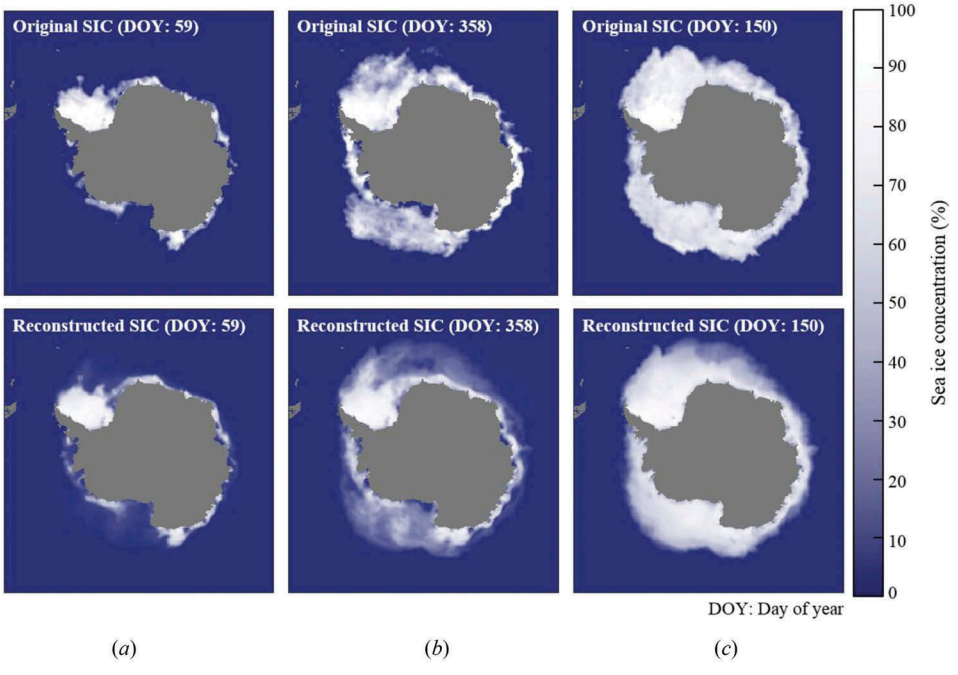

Figure 4. Comparison of the original sea ice concentration data with the reconstructed data. (a) Best fit (RMSE 3.6031%), (b) worst fit (RMSE 9.2356%) and (c) mean fit (RMSE 6.9464%).

spatial variability in the Antarctic. The sea ice has significantly increased in the Ross Sea, while the Amundsen Sea sector exhibits a negative trend (Parkinson and Cavalieri 2012). Due to these phenomena, the trend is noisy, and it is difficult to predict future trends.

The fractional abundances of the temporal EMs in this study also provide a unique capacity for summarizing Antarctic sea ice changes over multiple decades. To simplify investigating source components of the overall sea ice decrease/increase in the Antarctic, fractions of seven seasonal sea ice EMs are combined into a single component. Figure 5 illustrates yearly proportional changes using three seasonal Antarctic sea ice characteristics, 1) non-seasonal sea ice, 2) the open sea and 3) the sum of seven seasonal sea ice types, over three regions: 1) the entire Antarctic, 2) the Ross Sea and 3) the Amundsen Sea.

As shown in Figure 5(a), the slopes of three trend lines over the extent of sea ice in the whole of the Antarctic were less steep than those for the Ross and the Amundsen Seas, which indicates that none of the three temporal signatures was significantly affected by the overall sea ice increase in the Antarctic.

Sea ice in the Ross Sea has exhibited a more significant change in annual average than the southern hemisphere average has. As shown in Figure 5(b), year-round SIC in the Ross Sea exhibits a positive trend; however, the area of open water has not changed significantly, and seasonal SIC exhibits a negative trend. These data indicate that sea ice growing in the Ross Sea sector is attributable to non-seasonal sea ice rather than open water or seasonal sea ice.

Unlike the Ross Sea, the Amundsen Sea sector has exhibited statistically significant decreases in SIC. The TMA results show negative trends in both non-seasonal sea ice and

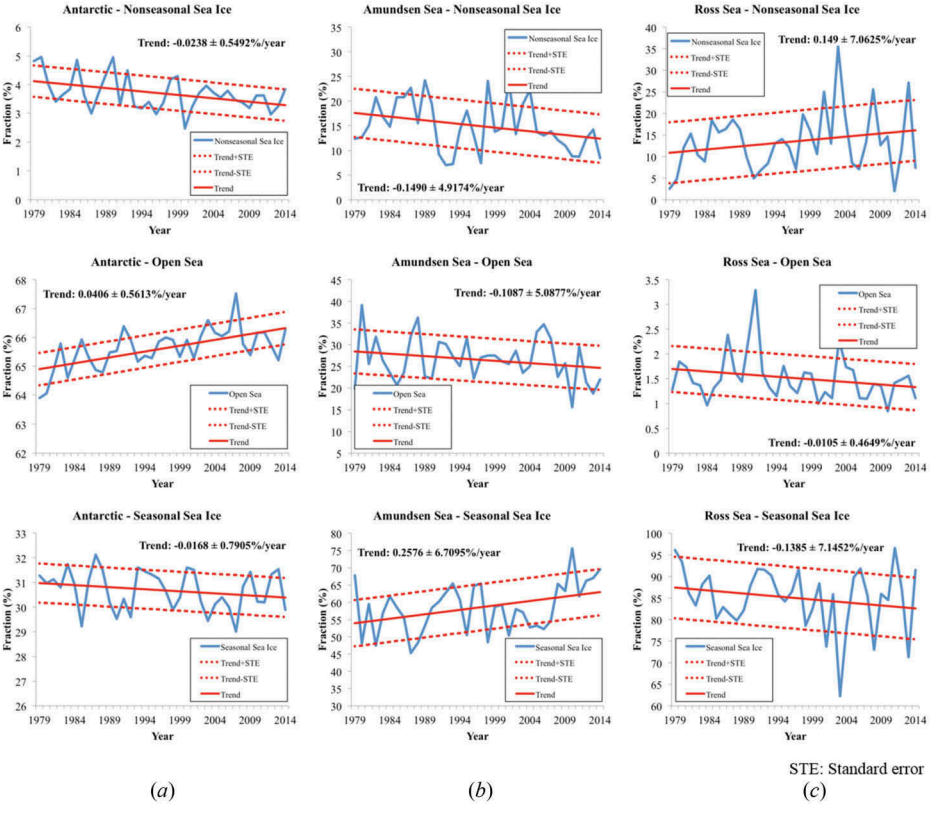

Figure 5. Regional comparison of non-seasonal sea ice, open water and seasonal sea ice in (a) the entire Antarctic, (b) the Ross Sea and (c) the Amundsen Sea.

open water in the Amundsen Sea. However, the trend for year-round sea ice shows a significant negative trend compared with the southern hemisphere and Ross Sea, while the extent of seasonal sea ice exhibits a positive trend (see Figure 5(c)). Overall, these results indicate that a decrease in the non-seasonal sea ice fraction in the Amundsen Sea directly affects the declining levels of sea ice, and considerable areas of year-round sea ice and sea ice-free regions in the Amundsen Sea have transitioned to areas of seasonal sea ice.

4. Conclusions

In this paper, TMA was applied in a combination of ML-based EE algorithm and fully constrained linear mixing model to decompose hypertemporal SIC data without incorporating prior knowledge. The representative temporal EMs were identified from 36 years of daily SIC data and then used to compute the fractional abundances of each temporal signal. Three conclusions were derived from this study. First, the 365 daily scenes were able to be reconstructed using a combination of several temporal EM signals and the corresponding abundance maps suggest that TMA efficiently provides a unique summary of long-term time series. Second, the reconstructed images did not frequently contain or minimize the impact of anomalies, which indicates that they can be used to detect changes. Lastly, the changes in fractional abundances for each temporal component in each region explained the overall impact of seasonal sea ice on the sea ice changes in each region. However, several challenges remain to motivate future research: 1) although we did not discuss problems associated with the quality of NSIDC's SIC data, the data should be calibrated with other sensors such as high-resolution optical data, or SIC retrieval algorithms should be compared and evaluated for more scientific purposes (Ivanova et al. 2015). 2) We applied only temporal information from HTIs to extract temporal EMs, discarding spatial information. Spatial information, however, provides distinguishing characteristics of image data; thus, using it should yield more accurate EM signatures. 3) An ensemble of the TMA results and other environmental factors might be used to better interpret sea ice dynamics in the Antarctic.

Note

1. Available at http://www.nsidc.org

Disclosure statement

No potential conflict of interest was reported by the authors.

Funding

This study was supported by the Korea Polar Research Institute [grant number PE15040] and the Ministry of Ocean and Fishery [grant number PM15040].

References

Bioucas-Dias, J. M., A. Plaza, N. Dobigeon, M. Parente, Q. Du, P. Gader, and J. Chanussot. 2012. "Hyperspectral Unmixing Overview: Geometrical, Statistical, and Sparse Regression-Based Approaches." *IEEE Journal of Selected Topics in Applied Earth Observations and Remote Sensing* 5 (2): 354–379. doi:10.1109/JSTARS.2012.2194696.

Cavalieri, D. J., C. L. Parkinson, P. Gloersen, and H. Zwally. 1996. *Sea Ice Concentrations From Nimbus-7 SSMR and DMSP SSM/I-SSMIS Passive Microwave Data, Natl*. Boulder, CO: Snow and Ice Data Center.

Cheriyadat, A., and L. M. Bruce. 2003. "Why Principal Component Analysis Is Not an Appropriate Feature Extraction Method for Hyperspectral Data." In 2003 IEEE International Geoscience and Remote Sensing Symposium, Toulouse, France, 3420–3422.

Chi, J., and M. M. Crawford. 2014. "Spectral Unmixing-Based Crop Residue Estimation Using Hyperspectral Remote Sensing Data: A Case Study at Purdue University." *IEEE Journal of Selected Topics in Applied Earth Observations and Remote Sensing* 7 (6): 2531–2539. doi:10.1109/JSTARS.2014.2319585.

DeFries, R. S., M. C. Hansen, and J. R. G. Townshend. 2000. "Global Continuous Fields of Vegetation Characteristics: A Linear Mixture Model Applied to Multi-Year 8 Km AVHRR Data." *International Journal of Remote Sensing* 21 (6–7): 1389–1414. doi:10.1080/014311600210236.

Green, A. A., M. Berman, P. Switzer, and M. D. Craig. 1988. "A Transformation for Ordering Multispectral Data in Terms of Image Quality with Implications for Noise Removal." *IEEE Transactions on Geoscience and Remote Sensing* 26 (1): 65–74. doi:10.1109/36.3001.

Haibo, B., and L. Ziwei. 2011. "Temporal Mixture Analysis in Monitoring Antarctic Sea Ice Concentration Variability." 2011 International Conference on Electronics, Communications and Control, Ningbo, September 9–11, 1696–1699.

Harsanyi, J. C., W. H. Farrand, and C.-I. Chang. 1993. "Determining the Number and Identity of Spectral Endmembers: An Integrated Approach Using Neyman-Pearson Eigen-Thresholding and Iterative Constrained RMS Error Minimization." The Thematic Conference on Geologic Remote Sensing, San Antonio, TX, February, 395–95.

Heinz, D. C., and C.-I. Chang. 2001. "Fully Constrained Least Squares Linear Spectral Mixture Analysis Method for Material Quantification in Hyperspectral Imagery." *IEEE Transactions on Geoscience and Remote Sensing* 39 (3): 529–545. doi:10.1109/36.911111.

Ivanova, N., L. T. Pedersen, R. T. Tonboe, S. Kern, G. Heygster, T. Lavergne, A. Sørensen, et al. 2015. "Satellite Passive Microwave Measurements of Sea Ice Concentration: An Optimal Algorithm and Challenges." *The Cryosphere Discussions* 9 (1): 1269–1313. doi:10.5194/tcd-9-1269-2015.

Keshava, N., and J. F. Mustard. 2002. "Spectral Unmixing." *IEEE Signal Processing Magazine* 19 (1): 44–57. doi:10.1109/79.974727.

Lobell, D. B., and G. P. Asner. 2004. "Cropland Distributions From Temporal Unmixing of MODIS Data." *Remote Sensing of Environment* 93 (3): 412–422. doi:10.1016/j.rse.2004.08.002.

Parkinson, C. L., and D. J. Cavalieri. 2012. "Antarctic Sea Ice Variability and Trends, 1979–2010." *The Cryosphere* 6 (4): 871–880.

Parry, M. L. 2007. *Climate Change 2007: Impacts, Adaptation and Vulnerability: Contribution of Working Group II to the Fourth Assessment Report of the Intergovernmental Panel on Climate Change*. Cambridge: Cambridge University Press.

Piwowar, J. M. 2008. "The Derivation of an Arctic Sea Ice Normal Through Temporal Mixture Analysis of Satellite Imagery." *International Journal of Applied Earth Observation and Geoinformation* 10 (1): 92–108. doi:10.1016/j.jag.2007.10.001.

Piwowar, J. M., D. R. Peddle, and E. F. Ledrew. 1998. "Temporal Mixture Analysis of Arctic Sea Ice Imagery: A New Approach for Monitoring Environmental Change." *Remote Sensing of Environment* 63 (3): 195–207. doi:10.1016/S0034-4257(97)00105-3.

Plaza, A., P. Martinez, R. Perez, and J. Plaza. 2004. "A Quantitative and Comparative Analysis of Endmember Extraction Algorithms From Hyperspectral Data." *IEEE Transactions on Geoscience and Remote Sensing* 42 (3): 650–663. doi:10.1109/TGRS.2003.820314.

Screen, J. A. 2011. "Sudden Increase in Antarctic Sea Ice: Fact or Artifact?" *Geophysical Research Letters* 38 (13). doi:10.1029/2011GL047553.

Winter, M. E. 1999. "N-FINDR: An Algorithm for Fast Autonomous Spectral End-Member Determination in Hyperspectral Data." SPIEs International Symposium on Optical Science, Engineering, and Instrumentation, Denver, CO, July 18, 266–275.

Yang, F., B. Matsushita, T. Fukushima, and W. Yang. 2012. "Temporal Mixture Analysis for Estimating Impervious Surface Area From Multi-Temporal MODIS NDVI Data in Japan." *ISPRS Journal of Photogrammetry and Remote Sensing* 72 (C): 90–98. doi:10.1016/j.isprsjprs.2012.05.016.